Surface effects in simulations of scanning electron microscopy images

Van Kessel, Luc; Hagen, Cornelis W.; Kruit, Pieter

DOI
10.1117/1.JMM.18.4.044002

Publication date
2019

Document Version
Final published version

Published in
Journal of Micro/ Nanolithography, MEMS, and MOEMS

Journal of
Micro/Nanolithography,
MEMS, and MOEMS

Nanolithography.SPIEDigitalLibrary.org

Surface effects in simulations of scanning electron microscopy images

Luc van Kessel
Cornelis W. Hagen
Pieter Kruit

SPIE.

Luc van Kessel, Cornelis W. Hagen, Pieter Kruit, "Surface effects in simulations of scanning electron microscopy images," *J. Micro/Nanolith. MEMS MOEMS* **18**(4), 044002 (2019), doi: 10.1117/1.JMM.18.4.044002.

Surface effects in simulations of scanning electron microscopy images

Luc van Kessel,* Cornelis W. Hagen, and Pieter Kruit
Delft University of Technology, Department of Imaging Physics, Delft, The Netherlands

Abstract

Background: Monte Carlo simulations of scanning electron microscopy (SEM) images ignore most surface effects, such as surface plasmons. Previous experiments have shown that surface plasmons play an important role in the emission of secondary electrons (SEs).

Aim: We investigate the influence of incorporating surface plasmons into simulations of low-voltage critical dimension SEM (CD-SEM).

Approach: We use a modified inelastic scattering model, derived for infinite flat surfaces, and apply it to nonflat, but smooth, geometries. This simplification captures most qualitative effects, including both surface plasmons and a reduced interaction with bulk plasmons near interfaces.

Results: We find that the SE signal hardly changes when surface interactions are turned on for a perpendicularly incident beam. When the incident beam is perfectly parallel to a surface, the SE signal does significantly increase. However, the beam must be extremely close to the surface for this effect to be appreciable. An SEM is unable to produce a beam that is both narrow and parallel enough to be noticeably affected.

Conclusions: The position of edges may appear shifted under specific circumstances. In realistic situations, it is unlikely to be a large effect.

 [DOI: 10.1117/1.JMM.18.4.044002]

Keywords: surface plasmons; scanning electron microscopy; Monte Carlo simulation.

Paper 19017 received Mar. 7, 2019; accepted for publication Oct. 14, 2019; published online Oct. 30, 2019.

1 Introduction

Scanning electron microscopy (SEM) is a standard tool for the inspection and metrology of semiconductor devices. It involves a focused electron beam scanning over a sample. The beam–sample interaction is a nontrivial process, producing secondary electrons (SEs) in a finite-sized interaction volume as well as backscattered electrons (BSEs). The interpretation of an SEM image is fairly straightforward if the features are large, but details of the beam–sample interaction become increasingly important as device features continue to shrink.

Semianalytical models for the SEM signal have been proposed,[1,2] but the most rigorous method in current use is Monte Carlo simulations.[3–6] These simulations attempt to predict the SEM image, assuming the sample geometry and material composition are known exactly. Starting from physical principles, they make broadly similar assumptions. An electron is treated as a classical point particle, scattering through the volume of a material in discrete events. The electron is treated as if it is in free flight between such events. The scattering probability per unit distance travelled $p(x)$ is given by an exponential distribution:

$$p(x) = \frac{1}{\lambda} e^{-x/\lambda}, \tag{1}$$

where λ is called the mean free path.

Two independent types of scattering are typically distinguished: elastic scattering, where an electron changes direction without losing energy; and inelastic scattering, where an electron loses energy and may excite an SE. Each of these mechanisms has its own mean free path. In addition, as an electron reaches a material interface, it may be reflected or refracted due to the change of inner potential between the materials.

The reflection and refraction of electrons at a surface is only one of the many effects that play a role at an interface. For example, there may be oxidation layers, dangling bonds, and contamination. Such highly sample-dependent effects are not considered in this work.

Instead, we correct the inelastic scattering mechanism for surface effects. An assumption that is often tacitly made is that elastic and inelastic scattering always behave as if the electron is deep inside bulk material. For scattering mechanisms that can be well described by electrons scattering on isolated atoms, such as inner-shell excitation or elastic Mott scattering, this is a valid approximation. For events where the electron probes the solid-state bulk, such as electron–phonon scattering or plasmon excitation, we may expect scattering behavior to be different near an interface.

Indeed, coincidence measurements[7–9] have provided evidence that surface plasmons may contribute significantly to SE emission when beam energies are on the order of 100 keV. Werner et al.[10] more recently performed a similar study at a beam energy (100 eV) close to low-voltage SEM.

*Address all correspondence to Luc van Kessel, E-mail: L.C.P.M.vanKessel@tudelft.nl

1932-5150/2019/$28.00 © 2019 SPIE

They find clear evidence for the contribution of surface plasmon decay to SE emission of similar magnitude to the volume plasmon. Neglecting surface plasmons in simulations of SEM images, as is typically done, may, therefore, not be acceptable.

The goal of this work is to study the sensitivity of simulated SEM images to the inclusion of surface plasmons.

We follow a framework similar to previous simulations of SEM images replacing the inelastic scattering mechanism by one where the material interface is explicitly taken into account.

This dielectric formalism includes surface plasmons as well as the "Begrenzung" effect, the reduced coupling strength to the volume plasmon near an interface. The goal of this work is to study the sensitivity of simulated SEM images to the inclusion of these effects.

We briefly mention the elastic and boundary scattering models used in Sec. 2. These are similar to what is currently in common use. Surface plasmons are introduced by replacing the inelastic scattering model. This is discussed in detail in Sec. 3. Results are shown in Sec. 4.

2 Scattering Models

For the energy range above 200 eV, we use Mott elastic scattering.[11] These scattering cross sections are obtained by solving the Dirac equation in a model potential near an atom. We use the ELSEPA program by Salvat et al.[12] to compute these scattering cross sections.

For energies lower than ~100 eV, the Mott description breaks down. As pointed out by Kieft and Bosch,[4] the electron's wavelength becomes comparable to interatomic distances. The picture of an electron scattering on a single isolated atom is no longer valid. A more technical issue is that the Mott scattering cross section becomes heavily dependent on assumptions in the model potential. Similar to Kieft et al., we use electron–acoustic phonon scattering for energies lower than 100 eV, based on the work of Schreiber and Fitting.[13] In the range 100 to 200 eV, we interpolate between acoustic phonon and Mott scattering.

As an electron crosses a material interface, it probes the difference of inner potential between the materials. This may cause the electron to be reflected or transmitted and refracted. We use a simple step function model potential to determine the transmission coefficient.

3 Surface Formalism

Typical modern simulations use the dielectric function to describe the inelastic scattering of electrons in matter. The strength of this approach is that the dielectric function can be measured in the optical regime. Assuming that all of space is occupied by a material with dielectric function $\epsilon(q,\omega)$ and that the electron is a single point charge, Maxwell's equations can be solved to find the induced electric field in the material. This electric field is oriented such that it slows down the electron, which is interpreted as inelastic scattering.

The result is an inelastic mean free path given by[14]

$$\lambda^{-1} = \frac{1}{\pi a_0 E}\int \mathrm{d}\omega \int \frac{\mathrm{d}q}{q}\,\mathrm{Im}\left[\frac{-1}{\epsilon(q,\omega)}\right], \tag{2}$$

where ω represents the energy loss, q is the momentum transferred, E is the primary electron's kinetic energy before the collision, and a_0 is the Bohr radius. Integration is over the kinematically allowed range. Probability densities for energy and momentum loss are given by $\lambda\partial\lambda^{-1}/\partial\omega$ and $\lambda\partial\lambda^{-1}/\partial q$, respectively.

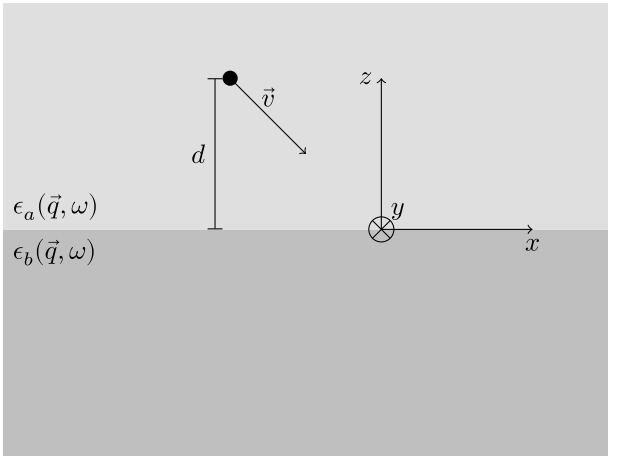

Fig. 1 Geometry used by Salvat-Pujol et al. Shaded areas represent the two materials, represented by dielectric functions $\epsilon_a(\vec{q},\omega)$ and $\epsilon_b(\vec{q},\omega)$. They are separated by the $z = 0$ plane. The electron moves with velocity $\vec{v}$ and passes through the origin at time $t = 0$.

In the general case, when not all of space is occupied by the same material, a similar analysis can be performed. However, the technicalities of solving the electric field are much more complicated. This has been done analytically for simple geometries,[15] such as infinite flat surfaces, wedges, or spheres.

For structures relevant to lithography, finding analytical solutions is impractical or impossible. A physically accurate alternative would involve numerically solving the induced electric field for every electron position, direction, and energy of interest. This parameter space is prohibitively large.

Instead, we make the following simplification. We use the analytically known solution for infinite flat surfaces and apply it to arbitrary geometries assuming that the radius of curvature in the geometry is sufficiently large everywhere. We will investigate the meaning of "sufficiently large" in more detail later.

We use the results from Salvat-Pujol and Werner.[16] A full derivation is given in that reference, we only repeat the main results. The situation is illustrated in Fig. 1. Materials with dielectric functions $\epsilon_a(\vec{q},\omega)$ and $\epsilon_b(\vec{q},\omega)$ fill the spaces $z > 0$ and $z < 0$, respectively. The electron moves with velocity $\vec{v}$. The electron's z coordinate is denoted as d, positive for region a, and negative for region b. At time $t = 0$, the electron passes through the origin.

Salvat-Pujol et al. solve this situation for a nonrelativistic electron by means of the image charge method. The assumption that the electron is not relativistic makes the problem formally electrostatic. Salvat-Pujol et al. remark that the usual boundary conditions for the electric and displacement fields at $z = 0$ are not restrictive enough to uniquely determine the image charges. Previous literature has chosen a variety of image charges to investigate the nonrelativistic case. Salvat-Pujol et al. parametrize the choice for image charges by the tuple of numbers (p_1, p_2, p_3), which can be set to (0, 1, 0) or (1, 1, 1) to reproduce earlier literature results.

The result is an inverse mean free path consisting of a bulk and a surface term: $\lambda^{-1} = \lambda_B^{-1} + \lambda_S^{-1}$. The surface term

captures both the surface plasmon coupling as well as the Begrenzung of the volume plasmon. The bulk term λ_B^{-1} is similar to Eq. (2), where ϵ_a or ϵ_b is selected depending on the sign of d. The surface interaction is given by

$$\begin{aligned}\lambda_S^{-1} = &-\frac{\hbar}{m_e a_0 \pi^2}\frac{|v_z|}{v}\int_0^{E/\hbar} \mathrm{d}\omega \int_{q_-}^{q_+} \mathrm{d}q \int_0^{\pi} \mathrm{d}\theta \sin\theta \\ &\times \int_0^{2\pi} \mathrm{d}\phi \frac{1}{q_\parallel^2 v_z^2 + (\omega - \vec{q}_\parallel \cdot \vec{v}_\parallel)^2} \\ &\times [\Theta(-t) e^{-q_\parallel |d|} + \Theta(t)\{2\cos[(\omega - \vec{q}_\parallel \cdot \vec{v}_\parallel)t] - e^{-q_\parallel |d|}\}] \\ &\times \mathrm{Im}\left\{ e^{i q_z d} f(\vec{q}_\parallel, \omega) \left[\frac{\Theta(d)}{\epsilon_a(\vec{q},\omega)} - \frac{\Theta(-d)}{\epsilon_b(\vec{q},\omega)} \right] \right\}. \end{aligned} \tag{3}$$

We use the notation that any vector $\vec{a}$ has components $\vec{a} = (a_x, a_y, a_z)$, the shorthand $a = |\vec{a}|$, and $\vec{a}_\parallel = (a_x, a_y)$ is the two-dimensional projection oriented parallel to the interface. Furthermore, $\vec{q} = q(\cos\phi \sin\theta, \sin\phi \sin\theta, \cos\theta)$, $\Theta(x)$ is the Heaviside step function, and

$$\frac{\hbar q_\pm}{\sqrt{2m_e}} = \sqrt{E} \pm \sqrt{E - \omega}, \tag{4}$$

$$k_z = \frac{\omega - \vec{q}_\parallel \cdot \vec{v}_\parallel}{v_z}, \tag{5}$$

$$f(\vec{q}_\parallel, \omega) = \frac{\frac{p_2}{\epsilon_b(\vec{q}_\parallel, k_z, \omega)} - \frac{1}{\epsilon_a(\vec{q}_\parallel, k_z, \omega)} + \frac{p_3}{\epsilon_b(\vec{q}_\parallel, -k_z, \omega)} - \frac{p_1}{\epsilon_a(\vec{q}_\parallel, -k_z, \omega)}}{\int_{-\infty}^{\infty} \mathrm{d}\kappa \frac{1}{q_\parallel^2 + \kappa^2} \left[\frac{1}{\epsilon_a(\vec{q}_\parallel, \kappa, \omega)} + \frac{1}{\epsilon_b(\vec{q}_\parallel, \kappa, \omega)} \right]}. \tag{6}$$

As before, the probability distributions of losing energy ω or momentum $\vec{q}$ are given by $\lambda \partial\lambda^{-1}/\partial\omega$ and $\lambda \partial\lambda^{-1}/\partial\vec{q}$.

We emphasise that λ_S^{-1} cannot be seen separately from λ_B^{-1}. λ_S^{-1} can be negative, representing a reduction in the bulk interaction. The sum $\lambda^{-1} = \lambda_B^{-1} + \lambda_S^{-1}$, however, must be positive.

We also note that λ_S^{-1} changes as the electron travels. λ^{-1} represents the scattering cross section in the electron's immediate environment, which is usually constant between successive events. This is not true in the present case, so λ can no longer be directly interpreted as the mean distance travelled between scattering events.

3.1 *Features of the Surface Correction*

A thorough discussion of the physical features contained in the surface formalism is already given by Salvat-Pujol and Werner.[16] For the reader's convenience, we repeat some of the main conclusions. We use the same dielectric function:

$$\frac{1}{\epsilon(q,\omega)} = 1 - \frac{\Omega_p^2}{\hbar^2 Z} \sum_{j=1}^{n} \frac{f_j}{\omega_j^2 + \hbar^2 q^4 / 4m_e^2 - \omega^2 - i\gamma_j \omega}, \tag{7}$$

with, for aluminum, $Z = 13$, $\Omega_p = 32.84$ eV, $n = 1$, $\hbar\omega_1 = 15.01$ eV, $f_1 = 3$, and $\hbar\gamma_1 = 0.5$ eV. This facilitates direct comparison to results shown by Salvat-Pujol et al.

Later on in this work, we will perform Monte Carlo simulations for silicon. For silicon, we use a more realistic dielectric function. We have obtained $\mathrm{Im}[1/\epsilon(q,\omega)]$ from measured data at $q = 0$,[17] which is extended into the $q > 0$ regime by means of the full Penn algorithm.[18] Our numerical implementation of the Penn algorithm follows the description of Shinotsuka et al.[19] The real part of $1/\epsilon(q,\omega)$ is then obtained by means of the Kramers–Kronig relation:

$$\mathrm{Re}\left[\frac{1}{\epsilon(q,\omega)}\right] = 1 + \frac{1}{\pi}\mathcal{P}\int_{-\infty}^{\infty} \frac{\mathrm{d}\xi}{\xi - \omega}\,\mathrm{Im}\left[\frac{1}{\epsilon(q,\omega)}\right], \tag{8}$$

where $\mathcal{P}$ stands for the principal value of the integral. We numerically evaluate this equation using the double Fourier transform method.[20]

Let us now consider an electron normally incident on a flat vacuum–aluminum interface. Figure 2 shows the differential inverse mean free path (DIMFP) with respect to energy $\partial\lambda^{-1}/\partial\omega$ for a 100-eV electron for several distances d to the interface. In Fig. 2(a), the electron is on the vacuum side; in Fig. 2(b), it is on the aluminum side.

When the electron is far on the vacuum side, it cannot lose any energy. However, as it approaches the interface, a peak appears near 11 eV, aluminum's surface plasmon energy. The surface plasmon coupling increases in strength as the electron closes in on the surface.

As soon as the electron moves to the aluminum side, a second peak appears beside the surface plasmon interaction. This second peak represents the volume plasmon of aluminum. As the electron moves deeper into the material, the surface plasmon coupling decreases in strength while the volume plasmon becomes stronger. This reduction of the volume

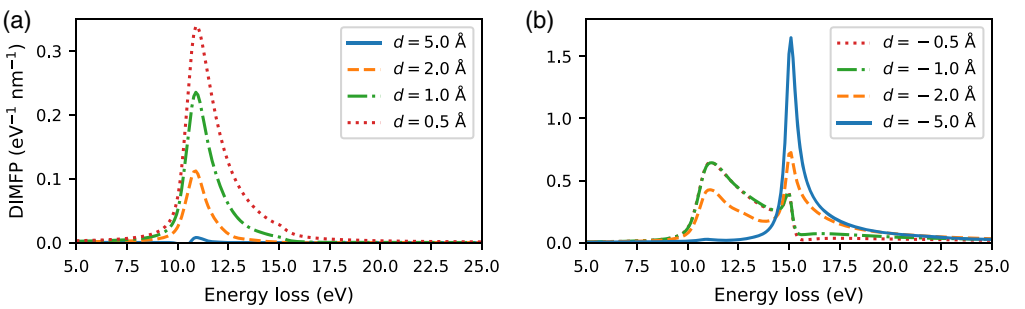

Fig. 2 DIMFP for a 100-eV electron, as a function of energy loss ω, for several distances d to a vacuum–aluminum interface. This represents the probability for an electron to lose a certain amount of energy, per unit distance travelled. The electron's direction is oriented from the vacuum toward the aluminum, along the surface normal. (a) electron on the vacuum side; (b) electron on the aluminum side. The $d = -0.5$ Å curve in (b) is hidden behind the curve for $d = -1$ Å.

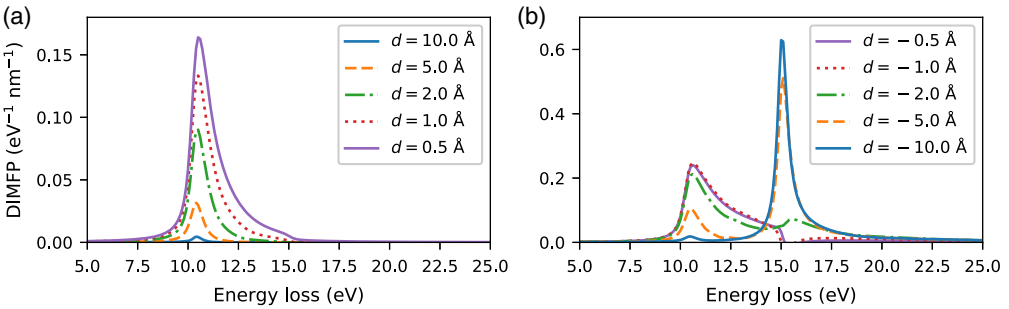

Fig. 3 Same as Fig. 2, for a 500-eV electron.

plasmon coupling near the interface is known as the Begrenzung effect. At a depth of 0.5 nm, the DIMFP is very similar to the bulk DIMFP.

Similar effects can be seen for a 500-eV electron (Fig. 3). For the purposes of this work, we want to note two things. First, the "surface layer" is somewhat thicker. For a 100-eV electron, the surface interaction becomes negligible at <5 Å from the interface. This interaction extends further for a 500-eV electron. In general, the surface layer is thicker for faster electrons. Second, the 500-eV electron has a lower interaction probability per unit distance travelled. This is a familiar effect also observed in bulk mean free paths.

We emphasise the extremely short range, in which the surface correction is relevant. Even for 500-eV electrons, the surface layer is less than a nm thick. Figures 2 and 3 show data for distances of 0.5 Å from the surface, much less than the distance between two atoms. The dielectric function is a continuum approximation to the microscopic response of the material, and whether it is a valid means to treat surface interactions at such small scales (low electron energies) is open for debate.

3.2 *Justification of the Infinite Flat Plane Approximation*

We have assumed that a curved geometry can be approximated as flat, if the curvature is smooth enough. This assumption needs to be justified, which we will do in two ways.

First, we show the lateral extent of the induced surface charge. In the work of Salvat-Pujol et al., there are three types of contributions to the electric field: the electron itself, its image charges in the bulk, and the induced surface charge. Clearly, if the geometry curves significantly on a scale where the surface charge is significant, the boundary conditions at the interface are not satisfied and the flat-plane approximation is wrong. Conversely, we may hope that if the interface curves far away from any significant surface charge, the boundary conditions at the interface are still approximately satisfied.

One might naively expect that the lateral extent of the surface charge is similar to the electron's distance from the surface. Since the surface interaction vanishes for distances less than a nm, one may expect the minimum radius of curvature to be similar. However, it is good to verify this.

Figure 4 shows the surface charge for 300 and 500 eV electrons, each 5-Å outside aluminum, moving directly toward the aluminum. This distance was chosen as it is the largest distance where the surface interaction is still noticeable. The surface charge can be seen to decay to almost zero within a few nm. When applying the surface formalism to

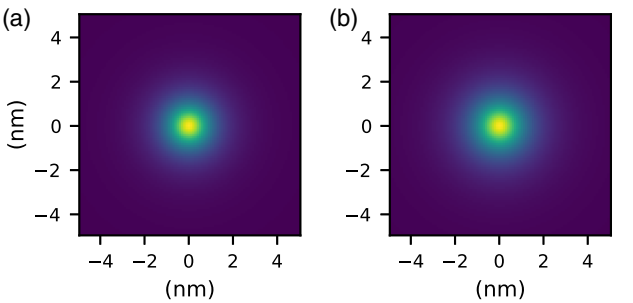

Fig. 4 Induced surface charge on a flat aluminum surface, for (a) a 300-eV and (b) a 500-eV electron. The electron is 5-Å outside the aluminum and travels toward the surface along the normal.

curved geometries, we will use electrons of ≤ 500 eV and a radius of curvature of at least 5 nm.

More justification comes from a numerical comparison to an analytical result for a curved geometry. García de Abajo[15] gave analytical expressions for several geometries. We choose the case of an electron passing outside a spherical nanoparticle.

It is well established that surface plasmons on spherical nanoparticles can behave qualitatively differently than on a flat plane. For a flat metallic plane in vacuum, the surface plasmon energy $\omega_s = \omega_p/\sqrt{2}$, where ω_p is the bulk plasmon energy. A nanosphere, however, can support a large spectrum of modes between $\omega_p/\sqrt{3}$ and $\omega_p/\sqrt{2}$. High-energy (of order 100 keV) electrons dominantly excite the low-order modes.

The situation is as follows. An electron starts infinitely far away from a sphere with radius a. It moves past the sphere with closest radius of passing $b > a$ and goes on to infinity. García de Abajo[15] then gave an expression for the "loss probability," given per unit of transferred energy. Its integral is the total probability that the electron loses energy.

With the flat-plane approximation, we can replicate this situation in a Monte Carlo fashion. We start the electron sufficiently far away from the sphere, tracking its energy as it passes the sphere, recording its final energy when it has moved sufficiently far away. This gives a distribution that is directly comparable, both in the distribution of energy lost and in terms of absolute value, to the analytical result.

The analytical result predicts that the low-order plasmon modes dominate when the electron energy is large and the electron passes far away from the sphere. García de Abajo confirmed this for the classic case of a 200-keV electron, and $(a, b) = (5, 6)$ nm or (10, 12) nm. However, as mentioned,

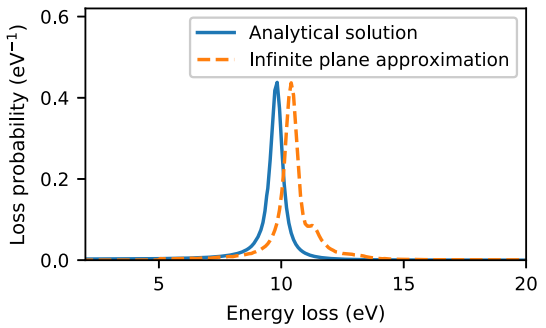

Fig. 5 Loss probability distributions for a 500-eV electron passing at $b = 10.5$ nm from a $a = 10$ nm aluminum sphere. This figure compares the analytical solution (blue curve) to the result from the flat-plane approximation (orange). Note the good agreement in absolute value.

the much lower-energy electrons considered in this work barely interact with surface plasmons at such distances from the surface. They need to pass much closer to the surface. In the analytical result, the low-order modes are then suppressed, and higher-order modes become more important.

We show numerical results for the energy-loss distribution in Fig. 5. The situation is a 500-eV electron, passing a sphere with $a = 10$ nm at a distance $b = 10.5$ nm. The low-order modes in the analytical result are suppressed and barely contributed to the peak in Fig. 5. Instead, the peak is caused by a combination of several higher-order modes. The amount of energy loss predicted by the analytical formula is slightly different from the flat-plane approximation. However, the agreement in absolute value is very good.

In conclusion, the amount of energy loss is slightly overestimated by the flat-plane approximation. However, the number of events is captured very well. The latter property is the most important for the purpose of SEM images.

3.3 *Monte Carlo Implementation*

The Monte Carlo implementation is not as straightforward as it is for bulk inelastic scattering. For bulk inelastic scattering from Eq. (2), one needs to store two- and three-dimensional tables. The two-dimensional table contains a probability distribution of energy loss, for each electron energy of interest. The three-dimensional table contains, for each electron energy and energy lost, a probability distribution of the momentum loss.

Surface inelastic scattering also depends on the electron's distance and angle to the surface, adding two dimensions to the tables mentioned above. In addition, we now need to sample two degrees of freedom for the momentum transfer. The bottom line is a need for 4-, 5-, and 6-dimensional tables: too large to fit in our computer's memory.

Therefore, we make the simplification that an inelastic event only causes the electron to slow down. We then only need a 4-dimensional table to sample the energy loss given the original energy, distance and angle to the surface.

We assume the following behavior for the creation of SEs. When an inelastic event takes place, an SE is created moving in a uniformly distributed random direction. If the primary electron lost energy ω, the SE's energy is $E_0 + \omega$. E_0 is determined from the probability distribution $P(E_0, \omega) \propto \sqrt{E_0(E_0 + \omega)}$, where E_0 is between 0 and the Fermi energy. This probability distribution is the product of the SE's densities of states before and after the excitation. If the primary electron is in vacuum, the SE is started on the mirrored side of the boundary, inside the material. We acknowledge that this model is very simplistic and that there is room for improvement.

What remains to be discussed is when an inelastic event takes place. Remember that the "mean free path" changes as a function of the electron's position. A random free path length sampled according to Eq. (1) is, therefore, only correct near the electron's starting position. This can be solved by introducing a "maximum step length" between successive scattering events. This maximum step length should be small enough, such that the mean free path barely changes over this distance. We have used 0.1 Å here, but a larger value is possible without significantly influencing the results.

If the free path sampled according to Eq. (1) is longer than this maximum, we travel precisely the maximum and sample a new free path length. This mechanism prevents steps between the "physical" elastic or inelastic events from getting too large and guarantees that the inelastic mean free path is suitably updated along the electron trajectory. Salvat-Pujol and Werner[16] did something similar, except their "null" event takes place stochastically with a mean free path $\lambda_{\min}$. This should lead to similar behavior in the limit that $\lambda_{\min}$ is much smaller than the elastic or inelastic mean free paths.

4 Results

4.1 *Backscattered and Secondary Energy Spectra*

We present the simulated reflection electron energy loss spectrum in Fig. 6. This was made for a 300-eV beam impinging perpendicularly on aluminum. Two simulations are shown: one with and one without surface effects enabled.

The energy spectrum without surface effects enabled is easily interpreted. The sharp peak at zero loss represents electrons reflected without losing energy. The strong peak at 15 eV represents electrons that have lost energy to a volume plasmon. Further peaks represent the excitation of multiple volume plasmons.

Enabling surface effects has a clear impact on the energy spectrum. The strong volume plasmon peak at 15 eV is reduced in absolute magnitude and is joined by the surface plasmon at ~11 eV. Subsequent peaks are caused by the excitation of multiple surface and/or volume plasmons. Clearly, if the backscattered energy spectrum is of interest, it is important that surface plasmons are taken into account.

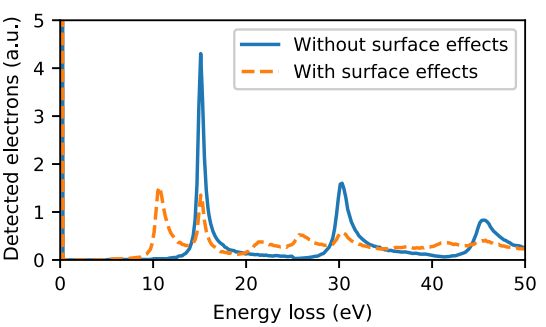

Fig. 6 Energy loss spectrum, for a 300-eV beam on aluminum. Simulations with (orange curves) and without (blue) surface effects enabled are compared.

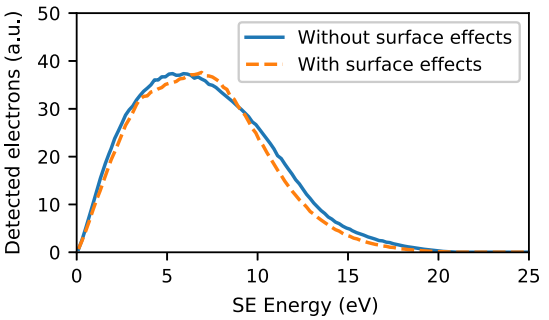

Fig. 7 SE energy spectrum, for the same simulation as Fig. 6. Simulations with (orange curves) and without (blue) surface effects enabled are compared. The material used is aluminum.

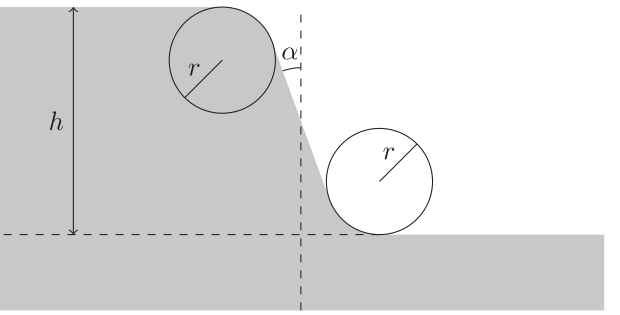

Fig. 9 Step geometry. The shaded area represents the silicon. The top and bottom corners are circular, and the wall may be angled.

The corresponding energy spectrum for SEs is presented in Fig. 7. The distinctive peaks in the energy loss spectrum of Fig. 6 are not visible. No additional "surface plasmon" peak is visible when surface effects are enabled in the simulation. This is because of our assumptions in the SE generation mechanism: SEs generated after surface plasmon decay are created inside the material and have to overcome the work function barrier to escape the material. The probabilistic transmission model mentioned in Sec. 2 effectively smooths out the features in the SE energy spectrum inside the material.

4.2 *Yields*

When taking SEM images, one is not typically interested in the detailed energy spectrum. Instead, detected electrons are counted, with only a very crude energy filter to distinguish between "secondary" (<50 eV) and "backscattered" (>50 eV) electrons. These yields—the average number of secondary or BSEs per incident electron—are shown in Fig. 8 for silicon, as a function of beam energy.

These yields are fairly similar to typical measured data[21] (not shown). Measured BSE yields saturate around 0.2. Measured SE yields tend to reach a maximum of 1.2 at a beam energy of ∼300 eV, but there is a large (factor 2) spread between various experiments. SE yields are influenced by, among others, surface oxidation, contamination, dangling bonds, and surface roughness. None of these effects are present in these simulations. Interestingly, we find that the SE yield is barely changed when our surface model is enabled.

Section 3.3 mentions several simplifications that may influence the SE yield. These include the energy and direction of SEs, as well as their starting position. It is possible that a different implementation gives a slightly different SE yield when surface effects are enabled. However, it is unlikely to change the general picture much.

4.3 *SEM Image*

We will now investigate the effect of introducing surface effects on an SEM image of a single silicon step (see Fig. 9). This step has circular rounded top and bottom corners to ensure smoothness. We vary the sidewall angle and electron beam energy. The electron beam is infinitely sharp, and we show only the SE signal.

We want to compare simulations with surface effects enabled and with surface effects disabled. We apply a vertical offset and linear scaling to the absolute SE yield, such that the signals overlap away from the edge. This facilitates comparison of the signals near the edge.

We show the case of a vertical sidewall in Fig. 10. The step height is 20 nm, the corner radius is 5 nm, and the beam energies are 300 and 500 eV. All SEM traces show the well-known enhancement of signal near the edge, which we will call the "edge blooming" effect in this work. When surface effects are enabled in the simulation, the SEM image taken at 300 eV shows a very sharp additional spike near the edge. This is a direct consequence of a somewhat pathological set of assumptions and parameters: the infinitely sharp electron beam travels at extremely close range ($x = 0.05$ nm) to the edge and is oriented perfectly parallel to the edge. The electrons travel on the vacuum side and are able to efficiently excite surface plasmons and the corresponding SEs, without being deflected.

No spike can be seen for 500-eV beam energy, though the SEM signal is slightly enhanced at $x = 0.05$ nm when surface plasmons are enabled. The fact that the spike is not

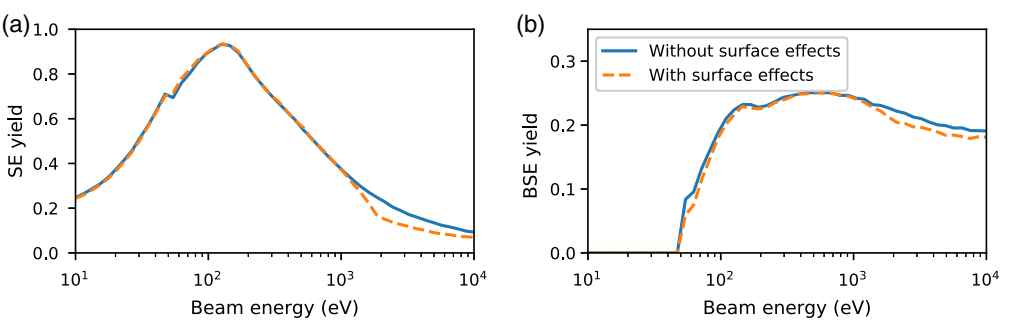

Fig. 8 (a) Simulated secondary and (b) backscattered yields, for simulations with (orange curves) and without (blue) surface effects enabled. The material used is silicon.

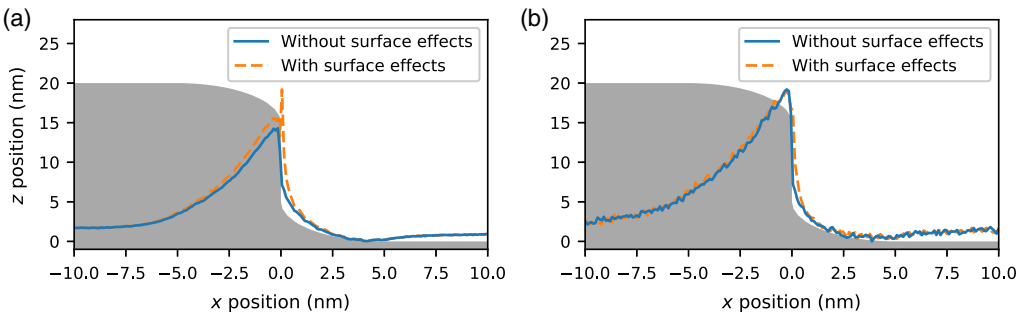

Fig. 10 SEM signals for a geometry with $h = 20$ nm, $r = 5$ nm, $\alpha = 0$ deg. Simulations with (orange curves) and without (blue) surface effects enabled are compared: (a) beam energy 300 eV and (b) beam energy 500 eV. The shaded area represents the silicon feature. The feature appears skewed because the axes are not equally scaled.

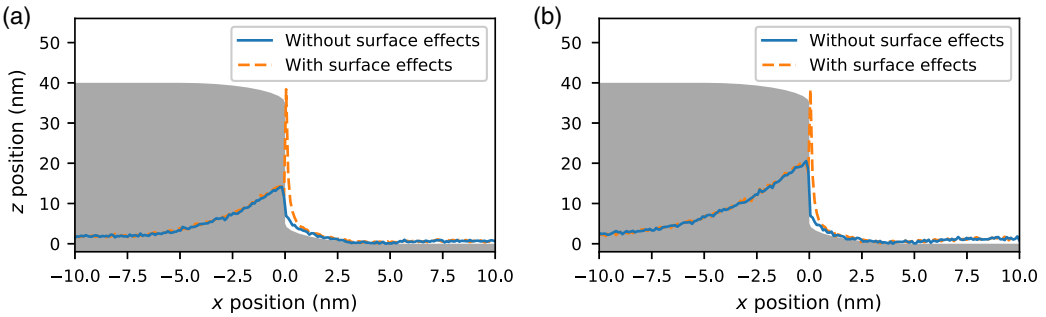

Fig. 11 Same as Fig. 10, for $h = 40$ nm.

present in the 500-eV linescan is due to the larger mean free path for these higher-energy electrons.

When the step height is increased to 40 nm (Fig. 11), a spike also appears in the 500-eV SEM signal. The spike for a 300-eV beam at a 40-nm step is even higher.

It is impossible to create the exact circumstances of Figs. 10 and 11 in a regular CD-SEM. Still, if it was possible to perform this experiment, we expect such spikes to appear. The magnitude of the spikes, however, is likely to be overestimated by our model. Remember that a "surface event" does not deflect the primary electron in this model. The slight deflection that the primary electron suffers in reality would rapidly steer it out of the very narrow surface layer.

A 5-deg sidewall angle (Fig. 12) eliminates the observed spike. Instead, the SEM signal from the sidewall is somewhat enhanced when the electron beam is set to 300 eV. Surface effects make almost no difference under a 500-eV beam.

A feature with 1-deg sidewall angle (Fig. 13) holds few surprises given the other results. The signal from the sidewall angle is enhanced, to a degree more extreme than seen in Fig. 12 but less than the spikes in Figs. 10 and 11. The simulation with surface effects enabled predicts that the signal at the sidewall exceeds the familiar "edge bloom" effect if the beam energy is low. As before, we expect the fact that the sidewall signal is enhanced to be true. The magnitude of the effect may be overestimated due to the contribution of multiple scattering events as well as the assumption that every surface plasmon decays to an electron.

The result in Fig. 13 is of interest to metrology. When surface effects are taken into account, the signal from the sidewall exceeds the "edge blooming" effect. This introduces a bias into the measured position of the edge.

There are multiple ways to measure the edge position in an SEM signal. A typical way is to take the position where the signal intensity is at 60% between the minimum and maximum. If the edge position is measured in this way, Figs. 10–12 correspond to a bias of 0.1 nm or less. In Fig. 13, however, the simulations with surface effects included

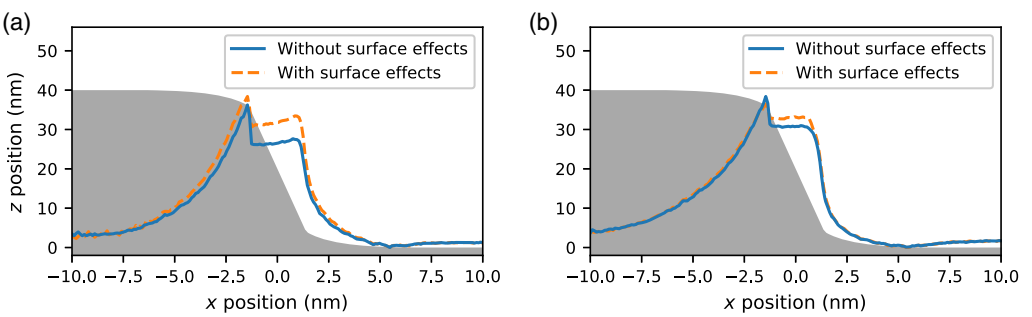

Fig. 12 Same as Fig. 10, for $\alpha = 5$ deg and $h = 40$ nm.

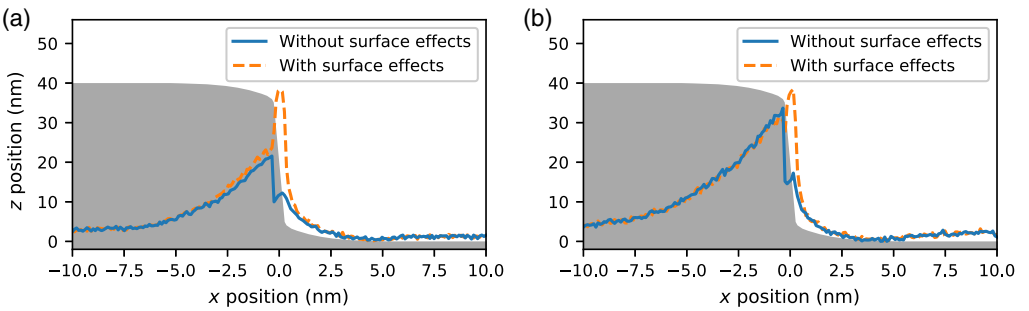

Fig. 13 Same as Fig. 10, for $\alpha = 1$ deg and $h = 40$ nm.

position the edge 0.6 nm further to the right than the corresponding simulations without surface effects included.

5 Discussion

At first glance, results obtained here appear to contradict experimental evidence mentioned in Sec. 1.[7–10] These experiments indicate that surface plasmon decay is an important contributor to SE emission.

The present simulations do not contradict these experiments. An SEM image counts the number of emitted SEs. As a consequence, information about the origin of SEs is lost.

Salvat-Pujol et al.[22] performed detailed coincidence experiments on aluminum and silicon. These experiments correlate the SE's energy to the energy lost by the primary electron. They compared these experiments to their Monte Carlo model, which is very similar to ours. They show that reasonable agreement between simulation and experiment can only be obtained if surface plasmon decay is included in the model.

In other words, the model captures the physics of SE generation by surface plasmon decay. In some situations, one has no choice but to include surface plasmons in the model. For the purpose of SEM images, however, they may be ignored.

6 Conclusions

The results shown above can be summarised as follows. Inclusion of surface effects in a Monte Carlo simulation leads to

- virtually no change in BSE yield,
- the SE yield changes only slightly,
- a changed BSE energy spectrum,
- a changed, but still mostly featureless, SE energy spectrum,
- a relative increase of the SE signal near a feature sidewall, which is largest for low landing energies.

Among others, we have assumed that incident electrons, upon coupling to a surface plasmon while in vacuum, do not change direction. We have also assumed that every surface plasmon decays to an electron–hole pair. These two assumptions lead to an overestimation of the amount, in which the SE signal is increased near a sidewall.

In some of the situations shown, the enhancement of the signal from the wall is so strong that the edge blooming effect is surpassed. It is unclear whether this is realistic. It would be difficult to observe this effect directly: the "wall feature" in Fig. 13 is likely to appear indistinguishable from the edge blooming effect.

If the enhancement of the signal from the sidewall is indeed as big as these simulations suggest, this can lead to a different assignment of the edge position when the SEM image is interpreted. Effectively, this position may shift from the "top" of the sidewall to the "bottom" side.

Surface effects have a much less significant influence on the SEM signal near the rounded top and bottom corners of our feature. We acknowledge that our corner radius is much larger than typical. However, under the present physical assumptions, decreasing this radius does not lead to more interesting features in the SEM signal.

It is possible that more interesting features arise when the flat-plane assumption is lifted and Maxwell's equations are solved for the actual geometry of interest. However, given that our present model captures most of the interesting features, we do not expect the qualitative conclusions to change much. The only interesting feature we observe, for the purposes of CD-SEM metrology, is an enhancement in signal from the sidewall angle. A more thorough treatment may, therefore, not be worth the effort.

Acknowledgments

This work is an updated version of "Surface effects in simulations of scanning electron microscopy images," Proceedings of SPIE, paper number 10959-29 (2019). The authors declare no conflicts of interest.

References

1. C. G. Frase, E. Buhr, and K. Dirscherl, "CD characterization of nanostructures in SEM metrology," *Meas. Sci. Technol.* **18**(2), 510–519 (2007).
2. C. A. Mack and B. D. Bunday, "Improvements to the analytical linescan model for SEM metrology," *Proc. SPIE* **9778**, 97780A (2016).
3. J. S. Villarrubia et al., "Scanning electron microscope measurement of width and shape of 10-nm patterned lines using a JMONSEL-modeled library," *Ultramicroscopy* **154**, 15–28 (2015).
4. E. Kieft and E. Bosch, "Refinement of Monte Carlo simulations of electron-specimen interaction in low-voltage SEM," *J. Phys. D Appl. Phys.* **41**(21), 215310 (2008).
5. Y. B. Zou et al., "Use of model-based library in critical dimension measurement by CD-SEM," *Measurement* **123**, 150–162 (2018).
6. T. Verduin, S. R. Lokhorst, and C. W. Hagen, "GPU accelerated Monte-Carlo simulation of SEM images for metrology," *Proc. SPIE* **9778**, 97780D (2016).
7. F. J. Pijper and P. Kruit, "Detection of energy-selected secondary electrons in coincidence with energy-loss events in thin carbon foils," *Phys. Rev. B* **44**(17), 9192–9200 (1991).
8. H. Mullejans et al., "Secondary-electron emission from magnesium oxide," *Philos. Mag. Lett.* **68**(3), 145–151 (1993).
9. M. R. Scheinfein, J. Drucker, and J. K. Weiss, "Secondary-electron production pathways determined by coincidence electron spectroscopy," *Phys. Rev. B* **47**(7), 4068–4071 (1993).

10. W. S. M. Werner et al., "Role of surface and bulk plasmon decay in secondary electron emission," *Phys. Rev. B* **78**(23), 1–4 (2008).
11. N. F. Mott, "The scattering of fast electrons by atomic nuclei," *Proc. R. Soc. London Ser. A* **124**(794), 425–442 (1929).
12. F. Salvat, A. Jablonski, and C. J. Powell, "ELSEPA—Dirac partial-wave calculation of elastic scattering of electrons and positrons by atoms, positive ions and molecules," *Comput. Phys. Commun.* **165**(2), 157–190 (2005).
13. E. Schreiber and H.-J. Fitting, "Monte Carlo simulation of secondary electron emission from the insulator SiO_2," *J. Electron. Spectrosc. Relat. Phenom.* **124**(1), 25–37 (2002).
14. R. H. Ritchie, "Plasma losses by fast electrons in thin films," *Phys. Rev.* **106**(5), 874–881 (1957).
15. F. J. García de Abajo, "Optical excitations in electron microscopy," *Rev. Mod. Phys.* **82**(1), 209–275 (2010).
16. F. Salvat-Pujol and W. S. Werner, "Surface excitations in electron spectroscopy. Part I: dielectric formalism and Monte Carlo algorithm," *Surf. Interface Anal.* **45**(5), 873–894 (2013).
17. E. D. Palik, *Handbook of Optical Constants of Solids, Five-Volume Set*, Elsevier, Amsterdam (1997).
18. D. R. Penn, "Electron mean-free-path calculations using a model dielectric function," *Phys. Rev. B* **35**(2), 482–486 (1987).
19. H. Shinotsuka et al., "Calculations of electron stopping powers for 41 elemental solids over the 50 eV to 30 keV range with the full Penn algorithm," *Nucl. Instrum. Methods Phys. Res. Sect. B* **270**(1), 75–92 (2012).
20. C. Peterson and B. W. Knight, "Causality calculations in the time domain: an efficient alternative to the Kramers–Kronig method," *J. Opt. Soc. Am.* **63**(10), 1238–1242 (1973).
21. D. C. Joy, "A database on electron-solid interactions," *Scanning* **17**(5), 270–275 (1995).
22. F. Salvat-Pujol, "Secondary-electron emission from solids: coincidence experiments and dielectric formalism," PhD Thesis, TU Wien (2012).

Luc van Kessel is a PhD student at Delft University of Technology. In 2014, he received his bachelor's degree in physics from Radboud University Nijmegen, followed by a master's degree in physics from the same university in 2017. His PhD work is on the simulation of electron-matter interaction with a particular focus on lithography applications.

Cornelis W. Hagen received his master's degree in 1983 and his PhD in 1991 of the Free University of Amsterdam, Netherlands. He was a researcher at the Paul Scherrer Institute in Switzerland from 1989–1992, and at the Kamerlingh Onnes Laboratory of Leiden University, Netherlands, from 1992–1994. In 1994 he joined Delft University of Technology as an assistant professor and was appointed as associate professor in 2008. His area of research is microscopy and lithography with charged particles.

Pieter Kruit is a full professor of physics at the Delft University of Technology in the Netherlands. He is a coauthor of over 150 publications in refereed international journals, author of 50 international patents, and supervisor of 30 PhD dissertations. He has had research programs on nanometer-resolution electron spectroscopy, low energy-spread electron and ion sources, and multibeam optics for microscopy and lithography.